Current Research (2025) Newfoundland and Labrador Department of Industry, Energy and Technology Geological Survey, Report 25-1, pages 183-203

DETRITAL ZIRCON U–Pb GEOCHRONOLOGY AND GEOCHEMISTRY OF OROSIRIAN SEDIMENTARY ROCKS, AILLIK GROUP, MAKKOVIK PROVINCE: IMPLICATIONS FOR PROVENANCE AND TECTONIC SETTING

S. Serna Ortiz, A.M. Hinchey and N. Rayner[1]
Regional Geology Section
[1]Geological Survey of Canada, 604 Booth Street, Ottawa, Ontario, K1A 0E8

ABSTRACT

The Paleoproterozoic Aillik Group of the Makkovik Province preserves evidence of sedimentation in a back-arc basin during the assembly of the supercontinent Nuna. This study integrates detrital zircon U–Pb geochronology and geochemistry to constrain the provenance and tectonic evolution of the Aillik Group. Provenance data indicate that sedimentation was primarily sourced from local Paleoproterozoic felsic volcanic rocks and Neoarchean to Paleoproterozoic sialic basement younger than the North Atlantic Craton (NAC). Maximum depositional ages suggest magmatism and back-arc extension persisted until ca. *1843 Ma. The shift in sedimentary provenance from predominantly local volcanic sources to a mixed source reflects progressive basin inversion and tectonic activity, likely coinciding with the onset of accretion of the Aillik–Cape Harrison Arc to the Kaipokok Domain. Additionally, the coeval timing of sillimanite-grade metamorphism and basin inversion (1843–1841 Ma) suggest the onset of collision occurring at this time. These findings refine the tectonic history of the Makkovik Province and suggest diachronous accretion along the broader Makkovik–Ketilidian orogen.*

INTRODUCTION

The Makkovik Province of Labrador records a complex Paleoproterozoic tectonic history characterized by arc formation, back-arc basin development, and subsequent inversion during the assembly of the supercontinent Nuna. The Aillik Group, part of the Adlavik Domain, represents a sedimentary and volcanic sequence that developed within a back-arc basin between *ca.* 1883 and 1848 Ma (Hinchey *et al.*, 2020; Hinchey, 2021b). Previous studies have focused on the stratigraphy, lithogeochemistry and isotopic characteristics of the Aillik Group, providing valuable insights into its depositional environment and tectonic setting (Hinchey, 2021a, b, c). Despite these advancements, questions remain regarding the provenance of the Aillik Group sediments, the timing and mechanism of basin inversion, and the tectonic processes leading to its eventual accretion to the Kaipokok Domain.

Detrital zircon studies are a valuable tool for understanding the provenance, depositional history, tectonic evolution and sedimentary processes recorded in sedimentary basins (Nelson, 2001; Cawood *et al.*, 2012; Barham *et al.*, 2022). The integration of detrital zircon data with other geological and geochemical proxies can provide a comprehensive understanding of the tectonic and sedimentary history of a region (Rothfuss *et al.*, 2012; Hu *et al.*, 2023). This study applies provenance analysis to the Aillik Group, utilizing detrital zircon U–Pb geochronology and sediment geochemistry to decipher its source characteristics and tectonic evolution. Integrating these data can constrain the sediment sources, depositional timing, and tectonic implications of the Aillik Group. This work underscores the broader utility of provenance studies in unravelling the complexities of ancient tectonic settings and sedimentary systems.

GEOLOGICAL SETTING

The Makkovik Province contains evidence of several tectonomagmatic events linked to arc collisions, the formation of back-arc basins, and their subsequent inversion, all occurring during the assembly of the supercontinent Nuna (Hinchey, 2021a). These geological processes highlight the complex tectonic history of the region. Based on the distribution of rock types, assemblages, and their correlation with the original zones proposed by Allaart (1976) for the Ketilidian orogen, it was divided into three domains, from west to east, the Kaipokok, Aillik and Cape Harrison domains (*see* Gower and Ryan, 1986; Kerr *et al.*, 1996). More recently, based on bedrock mapping in combination

with geochronological, lithogeochemical and isotopic data, Hinchey (2021b) merged the Aillik and the Cape Harrison domains into the Adlavik Domain, which correlates with the newly proposed Central Domain of the Ketilidian orogen (Steenfelt *et al.*, 2016; Bagas *et al.*, 2020; Hinchey, 2021b).

The Kaipokok Domain (Figure 1) consists of reworked gneiss of the Archean North Atlantic Craton (NAC) structurally overlain by passive margin and foreland basin metavolcanic and metasedimentary strata of the (2178 to ~2000 Ma) Post Hill and (>1850 Ma) Moran Lake groups that are collectively intruded by Paleoproterozoic granitoid intrusions (Kerr *et al.*, 1996; Barr *et al.*, 2001; Ketchum *et al.*, 2002). It records an early D_1 regional fabric related to thin-skinned thrusting and coeval amphibolite-facies metamorphism associated with the collision of the *ca.* 2100–2000 Ma Kaipokok Arc at *ca.* 1896 Ma and a D_2 fabric associated with subduction under NAC and emplacement of the (1895–1870 Ma) calc-alkaline Island Harbour Bay Plutonic Suite (IHBPS) in a dextral transpressive regime (Ketchum *et al.*, 1997; Culshaw *et al.*, 2000; Barr *et al.*, 2001). This domain is divided from the Adlavik Domain by several high-strain shear zones that collectively comprise the Kaipokok Bay Shear Zone (Ketchum *et al.*, 1997; Culshaw *et al.*, 2000).

The Adlavik Domain (Figure 1) comprises a variably deformed, felsic-dominated volcanic and sedimentary sequence (*ca.* 1883–1848 Ma Aillik Group), co-eval porphyritic granites (Measles Point Granite), (1815–1800 Ma) foliated plutons of the Cape Harrison Plutonic Suite, and multiple Paleoproterozoic intrusive suites (*ca.* 1800, *ca.* 1720 and *ca.* 1650–1640 Ma plutonic suite (Kerr, 1994; Ketchum *et al.*, 2002; Hinchey *et al.*, 2023). This domain is interpreted to record a rifted back-arc to composite arc formed on a continental ribbon between 1895–1848 Ma that collided against the accreted Kaipokok arc between 1836–1818 Ma, resulting in the inversion and subsequent northwestward thrusting of the Aillik Group recorded by the regional D_{3+4} thrusting and folding (D_{1+2} for the group) (Culshaw *et al.*, 2000; Hinchey, 2021c). The group preserves greenschist- to lower-amphibolite facies metamorphism and t*he term meta is omitted for brevity*. The stratigraphy of the Aillik Group is complicated by the repetition of units, caused by later folding and structural overprinting (D_5-D_6-D_7; Hinchey, 2013, 2021a; Hinchey *et al.*, 2020). Nevertheless, its thickness has been estimated between 7 and 15 km, from which at least 4.6 km correspond to siliciclastic strata (Hinchey, 2021a). Sedimentary facies in the Aillik Group comprise fine- to medium-grained sandstone and siltstone interbedded with clast-supported, massive conglomerates that record sedimentation along a high-energy coastline in a fan delta. In this context, conglomerates represent the subaerial part of the fan delta, whereas sandstones and siltstone represent the subaqueous to intermittently subaerial part (Hinchey, 2021a).

Detrital zircon U–Pb geochronology of this unit indicates provenance from local Paleoproterozoic sources and older basement rocks with ages between 2100–1900 and 2600–2300 Ma (Hinchey *et al.*, 2020). In addition, volcanic and felsic plutonic clasts in conglomerates of the Aillik Group suggest sources dominated by volcanic rocks and exposed igneous basement (Hinchey, 2021a). Notably, such igneous basement is not exposed in the Makkovik Province and is younger than the metamorphic 3262–2545 Ma basement exposed in the Hopedale block and presumed equivalents-aged gneiss in the Kaipokok Domain, although only two ages are reported at *ca.* 2878 and 2813 Ma (Ketchum *et al.*, 2002; Hinchey *et al.*, 2022).

METHODOLOGY

Detrital zircon U–Pb ages were obtained from four sedimentary samples from the Aillik Group between Cape Aillik and Aillik Bay (Figure 2, A-A') and near Wild Bight (Figure 2, transect B-B'). These samples when projected onto tectonostratigraphic columns built from cross-sections between Cape Aillik and Yetman's Cove and between Ford's Bight and Pomiadluk Point (Figure 3A, B), fall near the bottom and top of these columns. Descriptions of lithofacies associations, column thickness, and deformation along these sections are thoroughly described in Hinchey (2021a).

Geochemistry of three metasandstones and three metasiltstones of the Aillik Group from different parts of the Adlavik Domain (Figure 1) were obtained to understand the regional provenance variation within the Aillik Group. Two of these samples, corresponding to one metasandstone and one metasiltstone, were collected near Wild Bight (Figure 2) and near the same location of the detrital samples within the tectonostratigraphic column B-B' (Figure 3).

DETRITAL ZIRCON U–Pb GEOCHRONOLOGY

LA-ICP-MS

U/Pb and Pb/Pb isotopic rations of detrital zircons were obtained and measured by *in-situ* laser ablation using a GeoLas 193 nm excimer laser ablation system coupled to a ThermoFinningan ELEMENT XR magnetic sector-inductively coupled plasma-mass spectrometer (ICP-MS) at Memorial University of Newfoundland. Zircon grains were previously imaged by backscattered electron (BSE), and homogenous regions in the zircon grains free of complex internal zoning, cracks, and inclusions were ablated using a 10 μm bean rastered over the sample to create a 40 x 40 μm square spot. Laser fluence was set at 5 J/cm^2 with a pulse

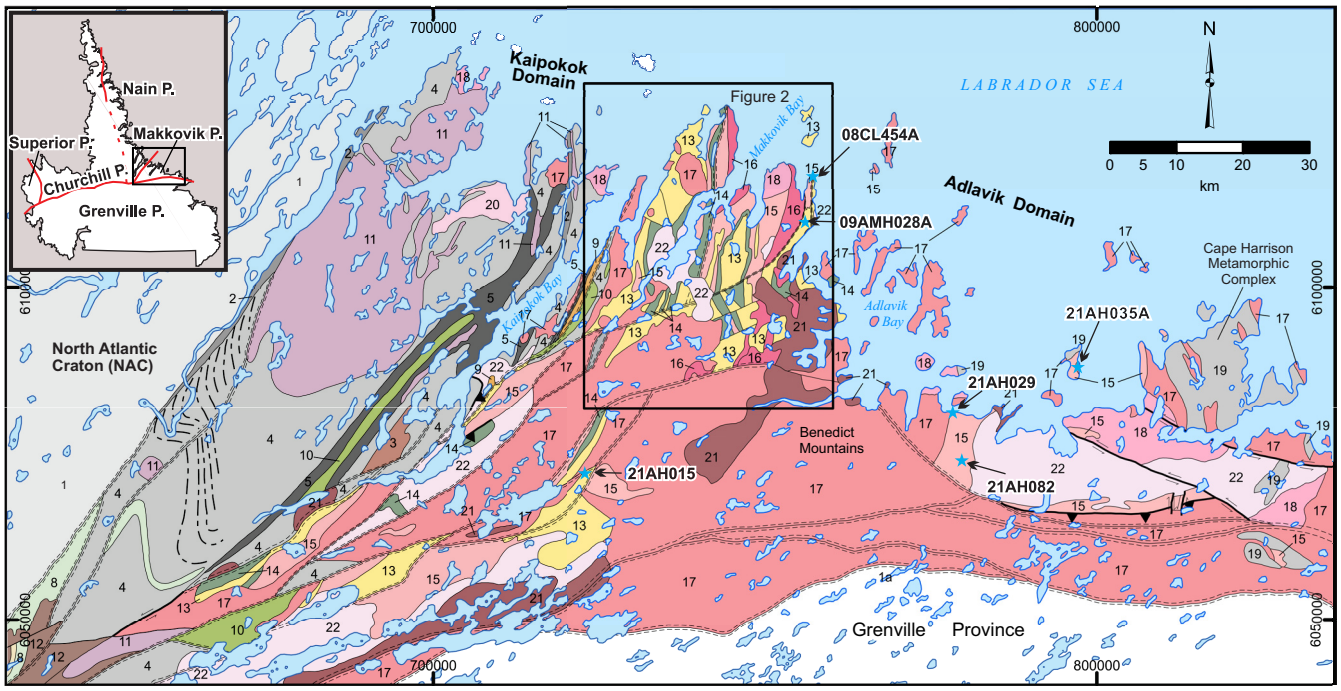

LEGEND

PALEOPROTEROZOIC

Stathenian (P_4 *ca.* 1800–1600 Ma)

Late Intrusions (P_4 *ca.* 1650–1635 Ma)

- 22 Granitic suites
- 21 Gabbroic suites

Mid Intrusions (P_4 *ca.* 1720 Ma)

- 20 Granitic suites

Orosirian (P_3 *ca.* 2150–1800 Ma)

Late Metamorphic Complexes (*ca.* 1810 Ma)

- 19 Cape Harrison Metamorphic Complex

Late Intrusions (*ca.* 1810–1780 Ma)

- 18 Unfoliated granitic suites
- 17 Foliated granitic suites

Mid Intrusions (*ca.* 1885–1840 Ma)

- 16 Syn-volcanic porphyries (MPGS)

Mid Supracrustals (*ca.* 1883–1848 Ma)

Aillik Group

- 15 Felsic volcanic rocks (rhyolite + felsic tuff)
- 14 Mafic volcanic rocks (basalt, minor mafic tuff)
- 13 Clastic sedimentary rocks

Unknown Group

- 12 Haggart Lake Formation (*ca.* 1850 Ma) (previously part of the Bruce River Group)

Early Intrusions (*ca.* 1890–1870 Ma)

- 11 Island Harbour Bay Plutonic Suite

Early Supracrustals (PHG ca. <2013 Ma)

Post Hill Group (PHG)

- 10 Metabasalt rocks
- 9 Psammitic to pelitic rocks

Moran Lake Group (age uncertain, assumed coeval with the PHG)

- 8 Basalt
- 7 Metamorphosed sedimentary rocks (shale + sandstone)

ARCHEAN

Paleoarchean (*ca.* 3800–3200 Ma) reworked in the Paleoproterozoic

Kaipokok Domain

- 6 Affinity unknown
- 5 Mylomitic + migmatitic orthogneiss (deformed *ca.* 1870–1780 Ma)
- 4 Reworked NAC (deformed *ca.* 1900–1870 Ma)
- 3 Banded amphilolite, reworked NAC
- 2 Mylonitic NAC gneiss in shear zone (reactivated *ca.* 1900–1870 and ca. 1870–1780 Ma)
- 1 Orthogneiss and minor amphilolite and paragneiss (Hopedale Block)

SYMBOLS

- Geological contact
- Geophysical lineament
- Shear zone
- Dextral fault
- Sinistral fault
- Thrust fault
- Geochemistry sample

Figure 1. *Lithotectonic units of the Makkovik Province showing the location of geochemistry samples. Modified from Hinchey (2021). Location of Figure 2 is outlined in black.*

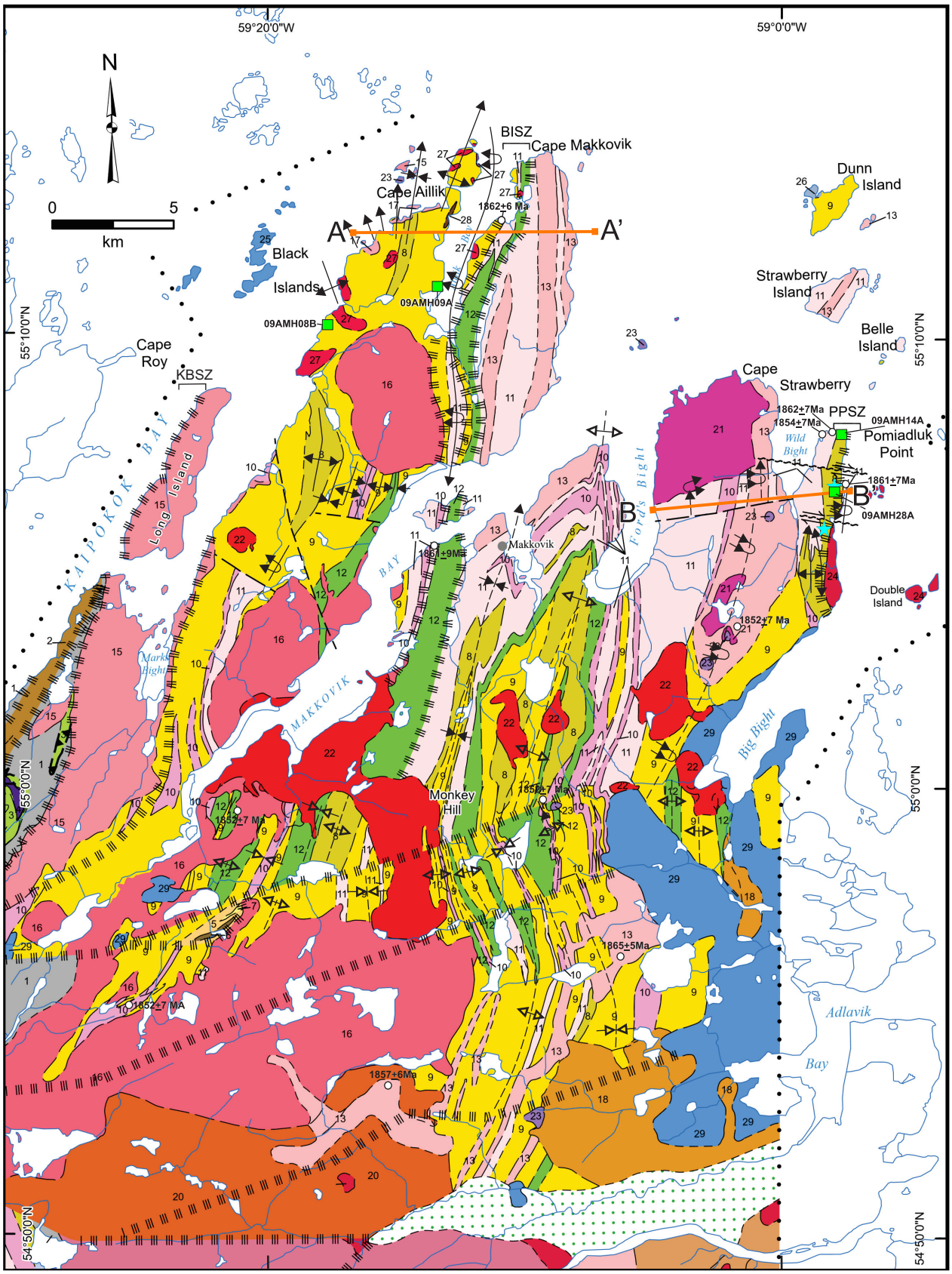

Figure 2. *Caption and Legend on following page.*

LEGEND

PLEISTOCENE–RECENT

30 Fluvioglacial, glacial gravel and sand

LATE PALEOPROTEROZOIC (*ca.* 1800–1640 Ma)

AGES POORLY CONSTRAINED (probably related to *ca.* 1650–1635 Ma magmatism)

29 Biotite-bearing gabbro

DYKES AND SILLS

28 Gabbro dykes

27 Granite dykes and sills

MESOPROTEROZOIC

LATE LABRADORIAN (*ca.* 1650–1640 Ma)

INTRUSIVE ROCKS

26 Monzodiorite and ferrosyenite

25 Leucogabbro

24 October granite

23 Leucogabbro (part of Adlavik Intrusive Suite)

22 Little Monkey Hill granite

EARLY LABRADORIAN (*ca.* 1720 Ma)

INTRUSIVE ROCKS

21 Cape Strawberry Granite (part of the Strawberry Intrusive Suite)

MID PALEOPROTEROZOIC (*ca.* 2100–1800 Ma)

STATHERIAN (*ca.* 1800 Ma)

INTRUSIVE ROCKS

20 Freshsteak granitoid

19 Big River granite (*ca.* 1802 Ma)

18 Lanceground Intrusive Suite

17 Biotite–muscovite leucogranite

16 Kennedy Mountain Intrusive Suite (*ca.* 1800 Ma)

15 Long Island Quartz Monzonite (*ca.* 1802 Ma)

14 Southern Numok Intrusive Suite (*ca.* 1808 Ma)

OROSIRIAN (*ca.* 1873–1850 Ma)

INTRUSIVE ROCKS

13 Foliated granite

SUPRACRUSTAL ROCKS (comprises the deformed and metamorphosed Aillik Group (*ca.* 1885–1848 Ma)

12 Metabasalt (amphibolite)

11 Banded felsic metatuff

10 Fine-grained feldspar, metarhyolite

9 Metasandstone

8 Metaconglomerate

7 Orthoquartzite

6 Banded iron formation

5 Semipelite–quartzite

RHYACIAN–OROSIRIAN (*ca.* 2100–1882 Ma)

INTRUSIVE ROCKS

4 Metagabbro

SUPRACRUSTAL ROCKS (includes part of the Post Hill Group)

3 Amphibolite (metabasalt)

2 Psammitic to pelitic schist

MESOARCHEAN (*ca.* 2800 Ma)

1 Orthogneiss

SYMBOLS

Limit of mapping

Contact (defined, approximate, assumed)

Fault (approximate, assumed)

Shear Zone

Synformal axis, antiformal axis (approximate)

Anticlinal axis, synclinal axis (defined, approximate, overturned)

Dextral fault (defined, approximate)

Sinistral fault (defined, approximate)

Thrust fault (approximate)

Zircon U-Pb age

Detrital zircon sample

Geochemistry sample

Figure 2. *Simplified geological map of the Monkey Hill and Makkovik area (NTS 13J/14, 13O/03 and parts of 13O/02). Modified from Hinchey (2021). KBSZ–Kaipokok Bay Shear Zone, PPSZ–Pomiadluk Point Shear Zone, BISZ–Big Island Shear Zone. Quoted zircon U–Pb ages, correspond to crystallization of volcanic rocks compiled from LaFlamme* et al. *(2013) and Hinchey* et al. *(2020).*

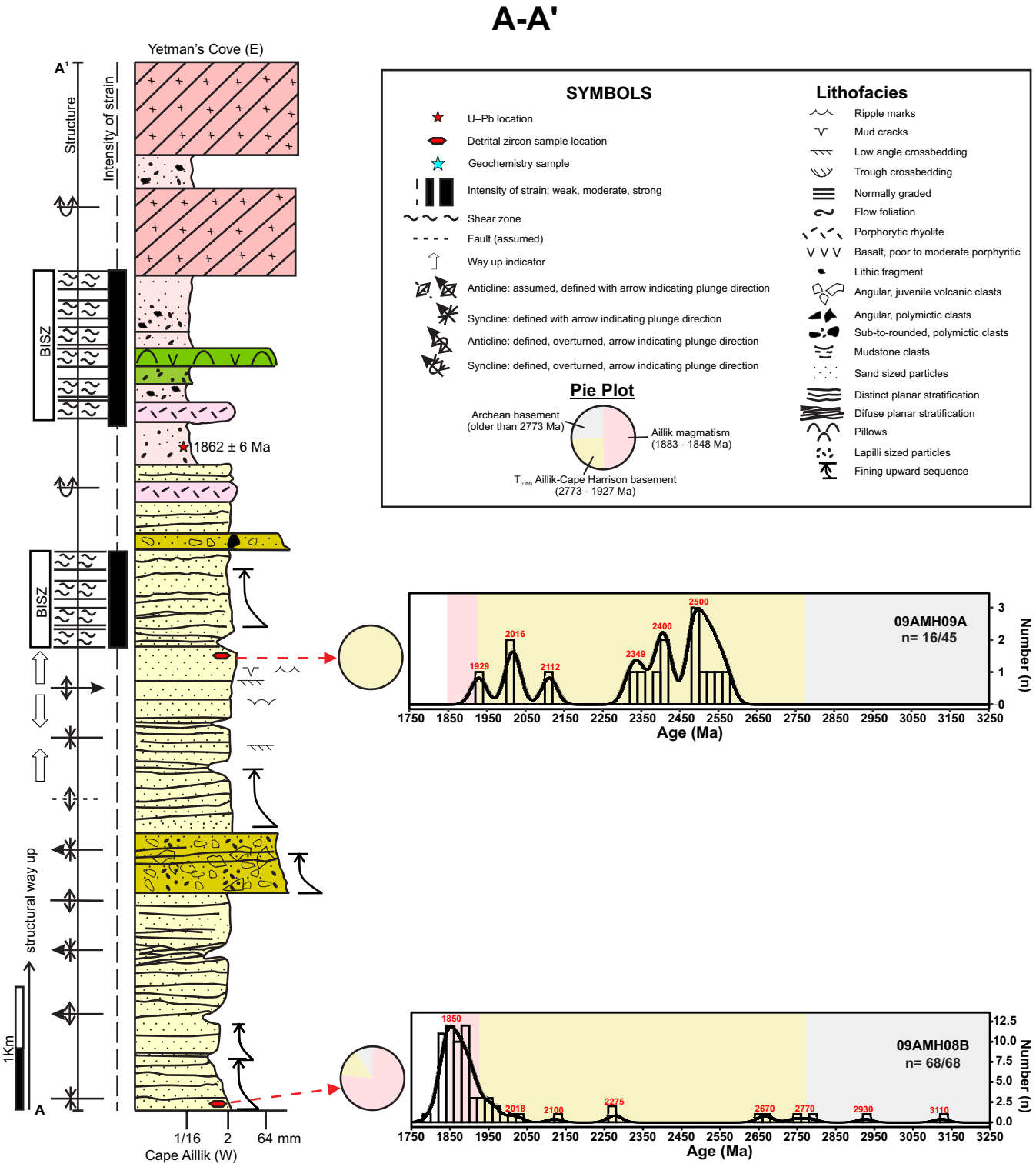

Figure 3. *Tectonostratigraphic columns showing lithofacies associations and KDE plots of two cross-sections within the Aillik Group, based on 1:50 000 scale map. Modified from Hinchey (2021). A) Cape Aillik to Yetman's Cove (Figure 2; A-A'); B) Ford's Bight to Pomiadluk Point (Figure 2; B-B'). BISZ–Big Island Shear Zone, PPSZ–Pomiadluk Point Shear Zone.*

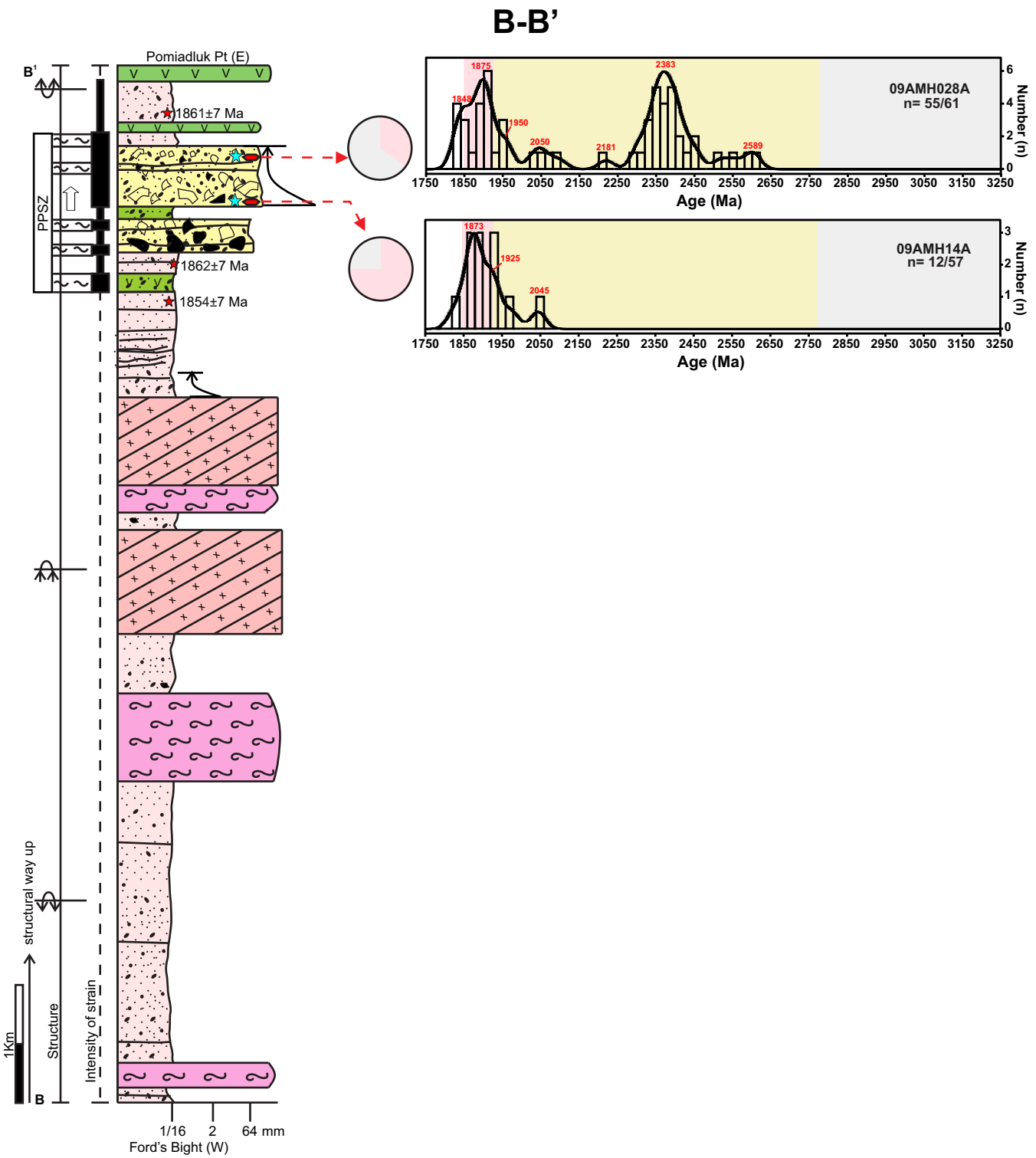

Figure 3 Continued. *Tectonostratigraphic columns showing lithofacies associations and KDE plots of two cross-sections within the Aillik Group, based on 1:50 000 scale map. Modified from Hinchey (2021). B) Ford's Bight to Pomiadluk Point (Figure 2; B-B'). BISZ–Big Island Shear Zone, PPSZ–Pomiadluk Point Shear Zone.*

rate of 10 Hz and 200 pulses with a total analysis time between 120 and 180 s. Raw data were corrected for the electron multiplier's dead time (20 ns) and processed offline in an Excel spreadsheet-based program (LAMdate; Košler *et al.*, 2002). For a detailed technique description, *see* Košler *et al.*(2002) and Cox *et al.* (2003). Data reduction included correction for gas blank, laser-induced elemental fractionation of Pb and U *via* the intercept method after Sylvester and Ghaderi (1997), and instrument mass bias. No common Pb correction was applied to the data. U concentrations were calibrated with Plešovice and 91500 zircon standards (Wiedenbeck *et al.*, 1995; Sláma *et al.*, 2008).

SHRIMP

Ion microprobe analysis of detrital zircon was performed using the SHRIMP II at the Geological Survey of Canada, following the procedure described by Stern (1997), with standards and U/Pb calibration methods following Stern and Amelin (2003). Zircon grains were cast in 2.5 cm diameter epoxy mounts along with fragments of the GSC laboratory standard zircon (z6266), which has a $^{206}Pb/^{238}U$ date of 559 Ma. Internal sections of the grains were exposed by grinding and polishing using 9, 6 and 1 μm diamond compound. The internal features of the zircon grains (such as zoning, internal domains, and alteration) were characterized by BSE imaging utilizing a Cambridge Instruments scanning electron microscope. Grain-mount surfaces were evaporatively coated with 10 nm Au of high purity. SHRIMP analyses were conducted using a 16O-primary beam projected onto the zircons at 10 kV. The sputtered area used for analysis was *ca.* 16–25 μm in diameter with a *ca.* 2–5 nA beam current. For the zircon analyses, the count rates of ten isotopes of Zr+, U+, Th+ and Pb+ were sequentially measured over 6–7 scans with a single electron multiplier and a pulse counting system that has a deadtime of 23 ns. Offline data processing was accomplished using customized in-house software. A 1σ external error for $^{206}Pb/^{238}U$ ratios reported in the data tables incorporates a ± 1.0% error in calibrating the standard zircon (*see* Stern and Amelin, 2003). No fractionation correction was applied to the Pb-isotope data; common Pb correction utilized the Pb composition of the surface blank (Stern, 1997).

Concordant values were calculated using the ratio of $^{206}Pb/^{238}U$ and $^{207}Pb/^{206}Pb$; analysis with excessive discordance (>5% discordant, >5% reverse discordant) were excluded from plots and interpretations. The reported ages for zircon grains older than 1000 Ma are based on $^{207}Pb/^{206}Pb$ (Supplementary data). Ages are reported at 1σ uncertainty and presented in Kernel density estimate (KDE) plots made with R.

Based on the lower analytical error of SHRIMP analyses compared to LA-ICP-MS analyses, samples 09AMH28A and 09AMH008B were combined and used to calculate the maximum depositional age (MDA) for the Aillik Group. This calculation was done using the Maximum Likelihood Age (MLA) algorithm of Vermeesch (2021), as it offers a most robust statistical approach compared to other MDA methods (Vermeesch, 2021).

MAJOR- AND TRACE-ELEMENT GEOCHEMISTRY

Major elements and some trace elements were analyzed by ICP-ES (inductively coupled plasma-emission spectrometry) following lithium borate fusion and multi-acid digestion. Other trace elements, including REE (rare-earth elements), were analyzed by a combination of ICP-MS (inductively coupled plasma-mass spectrometry) and INAA (Instrumental Neutron Activation Analysis).

All samples were prepared at the Geological Survey of Newfoundland and Labrador's Geochemistry Laboratory in St. John's, following protocols outlined by Finch *et al.* (2018). Major and select trace elements (Ba, Be, Cr, Sc, Zr) were determined by Inductively Coupled Plasma-Optical Emission Spectrometry (ICP-OES) following borate fusion. Volatiles were determined by loss-on-ignition (LOI) at 1000°C. Select trace elements, including As, Cd, Co, Cu, Li, Ni, Pb, Rb, V and Zn, were determined by ICP-OES following 4-acid digestion. REE and additional trace-element concentrations were determined by Inductively Coupled Plasma-Mass Spectrometry (ICP-MS) or INAA (Instrumental Neutron Activation Analysis) following borate fusion. Fluoride (F-) concentrations were determined by Ion-selective Electrode determination. Silver (Ag) concentrations determined by ICP-OES following digestion in nitric acid. Where an element was analyzed using multiple methods, the value determined by the most reliable method is presented. Details of geochemical methods, detection limits, and standard analytical errors for all the techniques applied are readily available from the relevant laboratories.

RESULTS

MAJOR-ELEMENT GEOCHEMISTRY

Samples from the Aillik Group show variable major-element composition with SiO_2 (58.0–72.3%, average 64.4%) and Al_2O_3 (11.5–19.9%, average 15.3) as the prevalent oxides, followed by K_2O (4.7–7.8%, average 6.4%), CaO (0.7–7.0%, average 4.3%), and $Fe_2O_3^T$ (2.6–6.3%, average 4%). Contents of other major elements are as follows: MgO (0.8–2.6, average 1.8%), Na_2O (0.2–2.6%, average 1.5), TiO_2 (0.2–0.5%, average 0.4%), MnO (0.1–0.3%,

average 0.1%), P_2O_5 (0.04–0.3%, average 0.1%). These samples have SiO_2/Al_2O_3 and $Fe_2O_3^T/K_2O$ ratios of 3.1–6.0 and 0.1–0.6, respectively, and plot between the wacke and the arkose fields (Figure 4). The CIA (Chemical Index of Alteration, $Al_2O_3/(Al_2O_3 + CaO^*+Na_2O+K_2O) * 100$, molar ratio; Nesbitt and Young, 1982), and ICV (Index of Compositional Variability, $(Fe_2O_3+K_2O+Na_2O+CaO^*+MgO+TiO_2)/Al_2O_3$, molar ratio; Cox *et al.*, 1995) values of the Aillik Group samples are 48.14–64.89 and 0.9–1.7, respectively (Table 1).

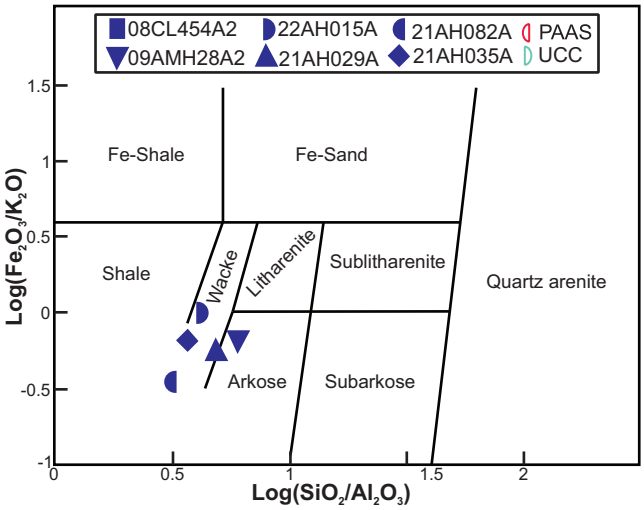

Figure 4. *Classification of sedimentary rocks from the Aillik Group (after Herron, 1988).*

TRACE-ELEMENT GEOCHEMISTRY

The Aillik Group samples show fractionated chondrite-normalized patterns with $(La/Yb)_N$ = 6.03–11.33 (average 8.71), negligible Ce anomalies (δCe = 0.95–1.11, average 1.03), and negative Eu anomaly (δEu = 0.35–0.78, average 0.51) on REE diagrams (Figure 5A, Table 2). On extended trace-element diagrams, samples are slightly enriched relative to the upper continental crust (UCC) and depict a flat pattern in the UCC-normalized spider diagram with negative Sr and Ti anomalies (Figure 5B).

DETRITAL ZIRCON GEOCHRONOLOGY

Samples 09AMH08B and 09AMH009A from Aillik Bay (Figure 2, A-A') yielded 68 and 16 single zircons ages that passed the discordance filter, respectively. Sample 09AMH08B consists of 3% Mesoarchean (3200–2800 Ma), 6% Neoarchean (2800–2500 Ma), 4% Rhyacian (2300–2050 Ma) and 87% Orosirian (2050–1800 Ma) ages. In contrast, sample 09AMH009A comprises 25% Neoarchean (2800–2500 Ma), 50% Siderian (2500–2300 Ma) and 6% Rhyacian (2300–2050 Ma) ages, and 19% Orosirian (2050–1800 Ma). KDE plots of these samples show contrasting modal distributions (Figure 3A), with sample 09AMH08B showing a polymodal distribution with a dominant peak at 1850 Ma and subordinate peaks at 2020, 2100, 2275, 2670, 2770, 2930 and 3110 Ma; whilst sample 09AMH009A depicts a polymodal distribution with minor peaks at *ca.*

Table 1. Major elements from sedimentary rocks of the Aillik Group

Samples **Datum: NAD27**	**21AH029A** **54.795883°N;** **58.665069°W**	**21AH035A** **54.857412°N;** **58.362305°W**	**21AH082A** **54.738035°N;** **58.647336°W**	**22AH015A** **55.110103°N;** **59.534129°W**	**09AMH28A2** **55.110103°N;** **58.966164°W**	**PAAS**	**UCC**
SiO_2	72.3	58.0	62.5	60.0	69.1	62.8	66.6
Al_2O_3	14.8	15.8	20.0	14.3	11.5	18.9	15.4
$Fe_2O_3(T)$	2.6	5.0	2.7	6.3	3.4	7.1	5.5
Fe_2O_3	1.7	1.6	1.1	3.9	2.6		
FeO	0.9	3.1	1.5	2.2	0.7		
FeO*	2.5	4.4	2.4	5.8	3.2		
MgO	0.8	2.6	1.5	2.6	1.7	2.2	2.5
CaO	0.7	6.0	1.2	7.0	6.4	1.3	3.6
CaO*	0.7	2.4	1.2	0.2	0.5		
Na_2O	2.5	2.6	1.5	0.2	0.6	1.2	3.3
K_2O	4.7	7.7	7.8	6.4	5.2	3.7	2.8
TiO_2	0.3	0.5	0.3	0.5	0.4	1.0	0.6
MnO	0.1	0.2	0.1	0.1	0.3	0.1	0.1
P_2O_5	0.0	0.1	0.1	0.3	0.1	0.2	0.2
LOI	1.6	1.5	2.2	1.1	0.9		
TOTAL	100.3	100.0	99.8	98.8	99.4		
SiO_2/Al_2O_3	4.9	3.7	3.1	4.2	6.0	3.3	4.3
Fe_2O_3/K_2O	0.4	0.2	0.1	0.6	0.5	1.9	2.0
ICV	1.0	1.7	0.9	1.3	1.3	1.1	1.6
CIA	58.7	48.1	60.4	64.9	60.2	69.4	52.8

NOTE: CaO*: CaO in silicate minerals (Nesbitt and Young, 1982; McLennan *et al.*, 1993)

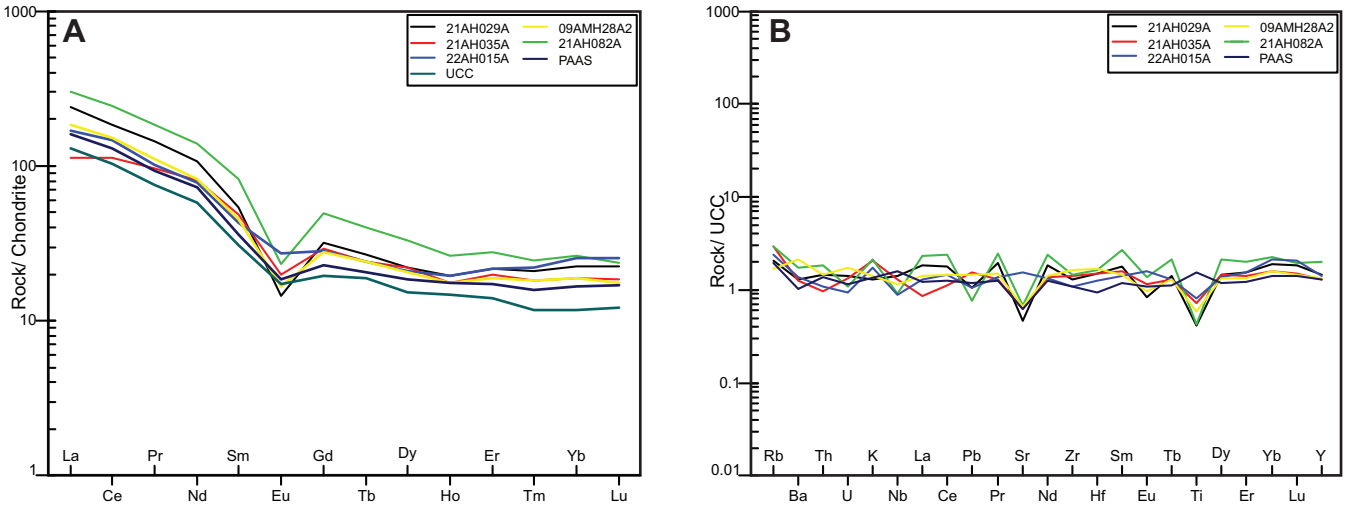

Figure 5. *Trace-element-normalized diagrams for the Aillik Group sedimentary samples. A) Chondrite-normalized diagram; B) Upper continental crust-normalized diagram. Chondrite data are from Sun and McDonough (1989), and the upper continental crust data are from Rudnick and Gao (2003).*

1930, 2020 and 2110 Ma and major peaks at *ca.* 2350, 2400 and 2500 Ma.

Samples 09AMH14A and 09AMH28A from Wild Bight (Figure 2, B-B') yielded 12 and 55 individual zircon ages that passed the discordance filter, respectively. Sample 09AMH14A is entirely defined by Orosirian (2050–1800 Ma) ages. Conversely, sample 09AMH28 consists of 7% Neoarchean (2800–2500 Ma), 42% Siderian (2500–2300 Ma), 7% Rhyacian (2300–2050 Ma) and 44% Orosirian (2050–1800 Ma) ages. KDE plot of the sample 09AMH14A depicts a polymodal age distribution with a dominant peak at *ca.* 1870 Ma and subordinate peaks at *ca.* 1925 and 2045 Ma (Figure 3B). KDE plot of sample 09AMH28A shows two dominant peaks at *ca.* 1875 and 2385 Ma with subordinate peaks at *ca.* 1850, 1950, 2050, 2180 and 2590 Ma. The maximum depositional age calculated using the MLA algorithm at 1σ for the Aillik Group yields 1843 ± 2.1 Ma.

DISCUSSION

The chemical composition of sedimentary rocks is controlled by several factors, including: A) chemical weathering of the source rock and diagenesis (Nesbitt and Young, 1982, 1984; Fedo *et al.*, 1995); B) sedimentary sorting during transportation and sedimentation (McLennan *et al.*, 1993); C) sedimentary recycling (Floyd and Leveridge, 1987; McLennan *et al.*, 1993); and D) provenance and depositional setting (Bhatia and Crook, 1986; Roser and Korsch, 1986). To confidently rely on the chemical signatures of sedimentary rocks to evaluate the provenance and depositional setting, it is necessary to evaluate the impact of weathering, sorting and recycling.

WEATHERING AND DIAGENESIS

Chemical weathering in humid climates is known to generate chemical and mineralogical changes in rocks and their weathered biproducts (Giovanoli *et al.*, 1988). Generally, sedimentary rocks derived from strongly weathered source rocks will have a marked depletion in mobile elements such as Na, Ca, K and Large Ion Lithophile Elements (LILE) relative to immobile elements such as Al, Ti, REE and High Field Strength Elements (HFSE). In rocks that are weakly weathered, the inverse relationship is expected (Nesbitt and Young, 1982, 1984).

Geochemical proxies, such as the Chemical Index of Alteration (CIA), assess the degree of weathering by evaluating the ratio of Al_2O_3 to alkalis (K_2O + Na_2O), which reflects feldspar breakdown (Nesbitt and Young, 1982). Typically, CIA values of ≤50 indicate fresh igneous rocks, while values nearing 100 represent residual clay (Nesbitt and Young, 1982; McLennan *et al.*, 1993). For Aillik Group sedimentary rocks, CIA values between 48–65 (Table 1) suggest weak weathering of the source area. However, because CIA is sensitive to K_2O variations, the effects of postdepositional processes, such as potassium metasomatism during diagenesis, must be evaluated to interpret these values accurately (Fedo *et al.*, 1995).

The Al_2O_3-CaO* + Na_2O-K_2O (A-CN-K) ternary diagram of Nesbitt and Young (1984) evaluates weathering trends of fresh igneous rocks *vs.* potassium metasomatism. Potassium metasomatism involves the addition of K_2O to aluminous clay, causing samples to deviate from ideal weathering trends toward the K_2O apex of the ternary dia-

Table 2. Trace elements compositions from meta-sedimentary rocks of the Aillik Group

Samples **Datum: NAD27**	**21AH029A** **54.795883°N;** **58.665069°W**	**21AH035A** **54.857412°N;** **58.362305°W**	**21AH082A** **54.738035°N;** **58.647336°W**	**22AH015A** **55.110103°N;** **59.534129°W**	**08CL454A2** **55.094983°N** **58.972441°W**	**09AMH28A2** **55.110103°N;** **58.966164°W**	**PAAS**	**UCC**
Ti	1606.7	2805.7	1654.6	3123.4	9334.9	2260.1	5993.0	3836.0
V	12.0	55.0	27.0	56.0	205.6	39.0	150.0	97.0
Cr	7.0	58.0	22.0	77.0	8.6	22.0	110.0	92.0
Co	3.0	7.0	6.0	11.0	34.8	11.0		
Ni	7.0	21.0	9.0	27.0	24.4	12.0	55.0	47.0
Cu	2.0	11.0	11.0	3.0		2.0		28.0
Zn	65.0	123.0	73.0	28.0	128.9	151.0		67.0
Ga	23.0	25.0	27.0	24.0		15.0		17.5
Ge		1.0	1.0	2.0		1.0	160.0	82.0
As	4.0	9.0	8.0	14.0	32.2	20.0		
Rb	168.0	241.0	238.0	196.0	79.1	140.0	160.0	82.0
Sr	149.0	202.0	221.0	494.0	499.7	212.0	200.0	320.0
Sc	6.8	9.9	7.6	11.6	28.1	5.5	16.0	14.0
Y	31.0	27.0	42.0	30.0	36.4	28.0	27.0	21.0
Zr	247.0	274.0	283.0	207.0		312.0	210.0	193.0
Nb	16.9	15.5	11.0	10.7	21.2	13.7	19.0	12.0
Cs	5.7	3.1	5.4	2.0		8.3	15.0	4.9
Ba	815.0	797.0	1084.0	872.0	1046.1	1324.0	650.0	628.0
La	56.9	26.9	71.1	40.4	39.2	44.1	38.2	31.0
Ce	113.3	69.6	149.0	90.5	94.0	92.7	79.6	63.0
Pr	13.8	9.1	17.6	9.7		10.6	8.8	7.1
Nd	49.8	37.5	65.6	36.4		38.6	33.9	27.0
Sm	8.3	7.4	12.5	6.6		6.9	5.6	4.7
Eu	0.8	1.2	1.4	1.6		1.0	1.1	1.0
Gd	6.5	6.0	10.1	5.8		5.7	4.7	4.0
Tb	1.0	0.9	1.5	0.9		0.9	0.8	0.7
Dy	5.6	5.6	8.4	5.3	7.0	5.2	4.7	3.9
Ho	1.1	1.0	1.5	1.1		1.0	1.0	0.8
Er	3.6	3.3	4.6	3.6		3.1	2.9	2.3
Tm	0.5	0.5	0.6	0.6		0.5	0.4	0.3
Yb	3.8	3.2	4.5	4.3		3.2	2.8	2.0
Lu	0.6	0.5	0.6	0.7		0.5	0.4	0.3
Hf	8.0	7.9	8.8	6.7		9.0	5.0	5.3
Pb	18.0	26.0	13.0	18.0	17.1	25.0	20.0	17.0
Th	15.4	10.3	19.2	11.5		15.3	14.6	10.5
U	3.8	3.6	2.9	2.5		4.7	3.1	2.7
Th/Sc	2.3	1.0	2.5	1.0		2.8	0.9	0.8
Zr/Sc	36.3	27.7	37.2	17.8		56.7	13.1	13.8
La/Th	3.7	2.6	3.7	3.5		2.9	2.6	3.0
Cr/Th	0.5	5.6	1.1	6.7		1.4	7.5	8.8
Cr/V	0.6	1.1	0.8	1.4	0.0	0.6	0.7	0.9
Y/Ni	4.4	1.3	4.7	1.1	1.5	2.3	0.5	0.4
Ti/Zr	6.5	10.2	5.8	15.1		7.2	28.5	19.9
La/Sc	8.4	2.7	9.4	3.5	1.4	8.0	2.4	2.2
∑REE	273.6	180.5	357.8	214.1	140.1	222.9	189.8	153.4
(La/Yb)N	10.7	6.0	11.3	6.7		9.9	9.7	11.1
(Gd/Yb)N	1.4	1.6	1.9	1.1		1.5	1.4	1.7
δEu	0.3	0.5	0.4	0.8		0.5	0.6	0.7
δCe	0.9	1.1	1.0	1.1		1.0	1.0	1.0

gram (Fedo *et al.*, 1995). In the Aillik Group samples, the A-CN-K plot shows deviation toward the K_2O apex, suggesting sediment sources experienced varying weathering conditions and were later altered by potassium metasomatism during diagenesis (Figure 6). When projecting the samples to the ideal granite weathering trend, the samples indicate weak to moderate chemical weathering, aligning partially with CIA values. The ICV values (0.9–1.7; Table 1) further support this interpretation, as values <1 suggest the presence of weathering products like kaolinite and illite, while values >1 indicate unweathered minerals such as amphibole, pyroxene, plagioclase and K-feldspar (Cox *et al.*, 1995). Overall, the Aillik Group sedimentary rocks record weak to moderate chemical weathering conditions.

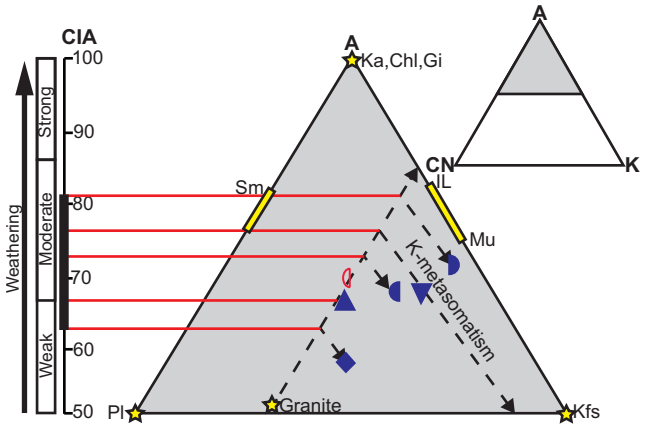

Figure 6. *A-CN-K plot of the Aillik Group sedimentary rocks (modified from Nesbitt and Young 1984). Granite composition is from Condie (1993).*

SEDIMENTARY SORTING

The mineralogical composition and chemical makeup of sedimentary rocks are influenced by the degree of sediment sorting that occurs during transportation and deposition (Pettijohn *et al.*, 1987; McLennan *et al.*, 1993). Sediment sorting can be evaluated using petrographic approaches that assess the textural maturity of the sedimentary rocks, considering factors such as grain size, shape, and the range of sizes present within the rock (Folk, 1951, 1980). Alternatively, geochemical proxies can also provide insights into the sorting processes. Ratios such as SiO_2/Al_2O_3 and Fe_2O_3T/K_2O reflect the relative abundance of quartz, clay minerals, feldspars, and ferromagnesian minerals in the sedimentary rocks (Potter, 1978; Herron, 1988). Additionally, the concentrations of REE can be associated with the presence of heavy minerals such as zircon, monazite, and allanite (McLennan *et al.*, 1993). These geochemical indicators demonstrate a direct correlation with the degree of sediment sorting. By examining both the petrographic and geochemical characteristics of sedimentary rocks, researchers can gain a more comprehensive understanding of the sorting processes that have influenced the final mineralogical and chemical composition of the sedimentary sequences.

The low SiO_2/Al_2O_3 and Fe_2O_3T/K_2O ratios (Table 1) for the Aillik Group samples indicate negligible sedimentary sorting. This is further illustrated in Figure 4, where samples plot between the wacke and the arkose fields. Furthermore, the similar REE concentrations of the Aillik Group samples compared to the UCC and post-Archean average Australia shale (PAAS) (Figure 5A, B) indicate limited enrichment in heavy minerals (*e.g.*, zircon, monazite, and allanite) because of sedimentary sorting.

SEDIMENTARY RECYCLING

Similar to the effects of sedimentary sorting, the process of sedimentary recycling can also influence the mineral composition and geochemical signatures of sedimentary rocks (Hubert, 1962; Sen and Mishra, 2023). Ultra stable and stable heavy mineral species, such as zircon and monazite, are often concentrated through sedimentary recycling, and their presence can be evaluated using geochemical proxies. The Zr/Sc ratio is commonly used as an indicator of zircon abundance, while the (Gd/Yb)N ratio reflects the presence of monazite (McLennan *et al.*, 1993). The Aillik Group sedimentary rocks exhibit higher Zr/Sc ratios (>14) and similar (Gd/Yb)N ratios (1–2) compared to the UCC and Post-Archean Australian Shale (PAAS) (Table 2), suggesting a slight enrichment in zircon. Further evidence of sedimentary recycling is provided by the Zr/Sc–Th/Sc binary plot (Figure 7), which compares a magmatic differentiation index (Th/Sc) against a zircon abundance index (Zr/Sc; McLennan *et al.*, 1993). In this plot, the Aillik Group samples plot along the sediment recycling trend, while the UCC and PAAS fall within the magmatic differentiation array. Based on these geochemical indicators, it is reasonable to conclude that the Aillik Group sedimentary rocks have undergone at least one cycle of sedimentary recycling, leading to the observed enrichment of ultra stable and stable heavy minerals.

PROVENANCE

Certain trace elements such as Th, Sc, Hf, Zr, Y, Cr, V, Ni and REE are generally considered immobile during weathering, diagenesis, and low- to medium-grade metamorphism (MacLean and Kranidiotis, 1987; Namayandeh *et*

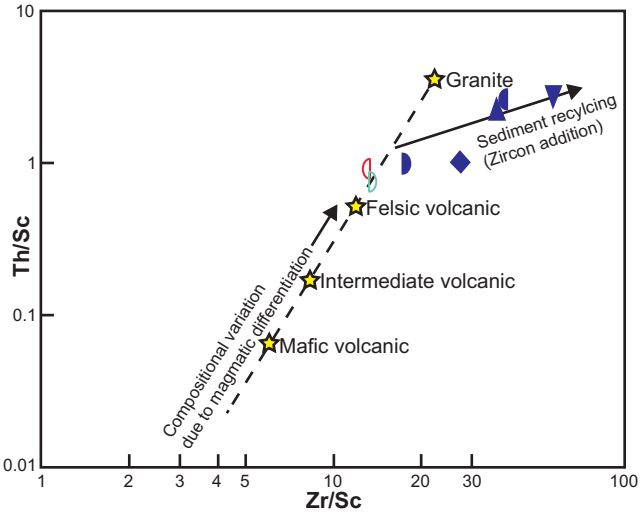

Figure 7. *Th/Sc* vs. *Zr/Sc plot of the Aillik Group sedimentary rocks (modified from McLennan* et al.*, 1993).*

al., 2020). As a result, their concentrations in sedimentary rocks are primarily influenced by the composition of the source rock (Bhatia and Crook, 1986; McLennan *et al.*, 1993). Mafic and felsic igneous rocks exhibit distinct REE concentrations and Eu anomalies. Typically, mafic igneous rocks are characterized by lower total REE abundances and the absence or minimal presence of Eu anomalies, whereas felsic rocks have higher total REE abundances and negative Eu anomalies (Cullers *et al.*, 1997 and references therein). The Aillik Group sedimentary samples display moderate to high REE contents (∑REE: 180–358 ppm), suggesting a dominant felsic igneous source. Furthermore, the highly fractionated REE patterns and the negative Eu anomalies observed in all the Aillik Group samples (Figure 5B) indicate an evolved magmatic source that likely underwent feldspar fractionation (McLennan *et al.*, 1993). This precludes a significant contribution from mafic igneous rocks in the source area.

Mineral phases in mafic igneous rocks, such as pyroxene and olivine, are commonly enriched in compatible elements like Sc, Cr, V and Ni. Conversely, incompatible elements like Th, Hf and Zr are preferentially concentrated in the melt during magmatic differentiation, leading to their enrichment in felsic igneous rocks (McLennan and Taylor, 1991; Rollinson, 1993). As a result, sedimentary rocks derived from mafic igneous sources are expected to display elevated contents of compatible elements, while those derived from felsic igneous sources would be enriched in incompatible elements (Bhatia and Crook, 1986; McLennan *et al.*, 1993). Furthermore, ratios such as La/Sc, Th/Sc, Cr/Th, La/Co and Th/Co, can be used to discriminate between sediment sources, as these ratios differ between mafic and felsic igneous rocks (Condie and Wronkiewicz, 1990; Cullers, 1994).

For the Aillik Group sedimentary samples, the contents of Sc, Cr, V and Ni are all lower than the mean MORB (mid-oceanic ridge basalt) values (Table 2 *vs.* Table 1, Gale *et al.*, 2013) and comparable to average granite compositions (Table 1, Shi *et al.*, 2011). Additionally, the La/Sc, Th/Sc, Cr/Th, La/Co and Th/Co ratios of the Aillik Group sedimentary rocks fall within the range typical of sedimentary rocks derived from felsic sources (Table 3). A felsic source composition is further supported by the Th/Sc–Cr/Th and Cr/V–Y/Ni binary plots (Figure 8A, B), which also indicate that the Aillik Group sedimentary rocks were primarily derived from the erosion of felsic igneous rocks.

Regional mapping in the Adlavik Domain has identified felsic volcanic rocks in conformable contact with sedimentary rocks of the Aillik Group (Hinchey, 2013). Reported crystallization ages for these volcanic rocks fall between

Table 3. Aillik Group sedimentary rocks ratios compared to rations of sandstones derived from felsic and mafic rocks

Sample ID	La/Sc	Th/Sc	Cr/Th	La/Co	Th/Co
21AH029A	8.37	2.26	0.45	18.97	5.13
21AH035A	2.72	1.04	5.63	3.84	1.47
21AH082A	9.36	2.53	1.15	11.85	3.2
22AH015A	3.48	0.99	6.7	3.67	1.05
08CL454A2	1.39			1.13	
09AMH28A2	8.02	2.78	1.44	4.01	1.39
Sandstones derived from felsic sources[1]	2.50–16.3	0.84–20.5	4–15.0	1.80–13.8	0.67–19.4
Sandstones derived from mafic sources[1]	0.43–0.86	0.05–0.22	25–500	0.14–0.38	0.04–1.40

[1]Cullers (1994, 2000); Cullers and Podkowyrov (2000); Cullers *et al.* (1998)

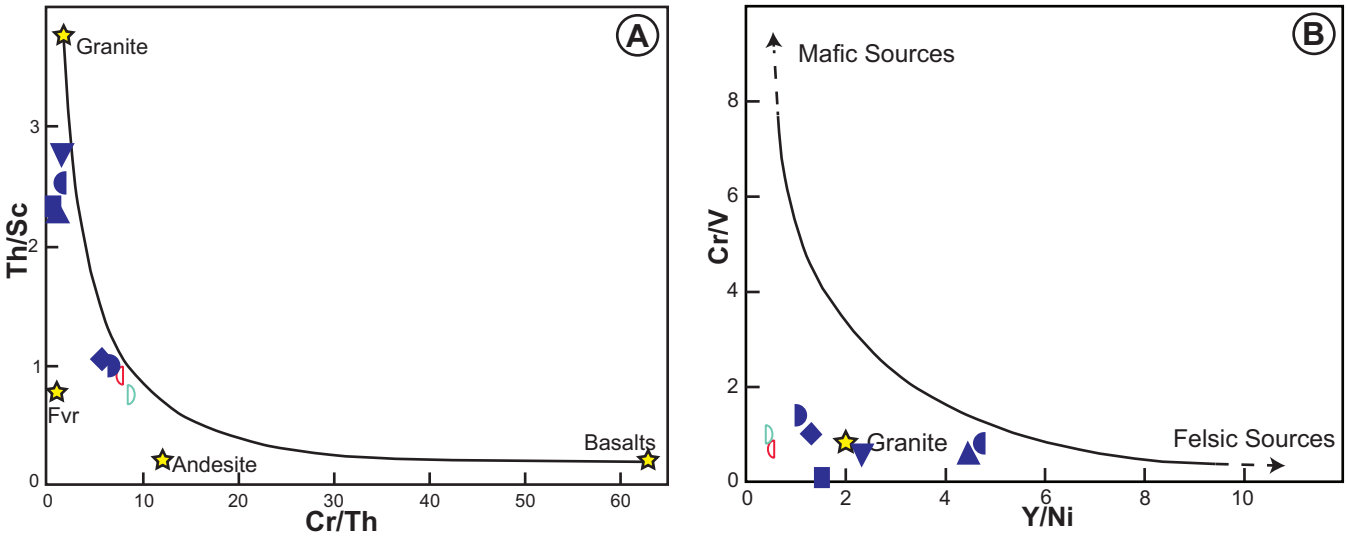

Figure 8. *Source rock discrimination diagrams for the Aillik Group sedimentary rocks. A) Th/Sc* vs. *Cr/Th plot; B) Cr/V* vs. *Y/Ni diagram (modified from McLennan* et al.*, 1993).*

1883 and 1848 Ma (LaFlamme *et al.*, 2013; Hinchey *et al.*, 2020), which are equivalent to the detrital zircon U–Pb age results obtained for the Aillik Group sedimentary rocks (Figure 3A, B). This suggests a close temporal relationship between the volcanic and sedimentary components. Furthermore, the poor compositional maturity and sorting of the Aillik Group sedimentary rocks (as discussed previously) indicate near-source deposition, rather than significant transport and reworking. This is supported by the geochemical signature of the sediments, which points to a felsic igneous rock provenance. Taken together, the field relationships, the near-source characteristics of the sediments, the geochemical evidence for a felsic igneous source, and the similar age distribution compared to the volcanic rocks within the Aillik Group, all suggest that the sedimentary rocks of the Aillik Group were primarily derived from the erosion of local felsic volcanic and plutonic rocks.

The Aillik Group sedimentary rocks contain detrital zircon grains with U–Pb ages older than 1890 Ma, but these older ages do not have known exposed sources within the Adlavik Domain. However, calculated Nd model ages $T_{(DM)}$ from the felsic volcanic rocks of the Aillik Group and synvolcanic intrusions (in part the Measles Point Granite) suggest the presence of an older sialic basement with ages between 2770 and 2160 Ma, as well as some less abundant juvenile crust as young as 1930 Ma (LaFlamme *et al.*, 2013; Hinchey, 2021b). Thus, the exhumation and erosion of this older basement could explain the zircon U–Pb ages between 2773 and 1927 Ma observed in the Aillik Group samples. Alternatively, the ages between 2100 and 1927 Ma could have been derived from remnants of the (2100–1900 Ma) Kaipokok Arc, which was already accreted to the NAC margin (Hinchey, 2021c). Sourcing from the established Kaipokok Domain could also explain the presence of Archean >2773 Ma zircon grains in sample 09AMH008B, which could have been derived from the passive margin strata of the nearby Post Hill Group or the reworked NAC (Ermanovics, 1993; Ketchum *et al.*, 2001). However, this provenance interpretation implies a link between the Aillik Basin and the Kaipokok Domain. Multiple tectonic models for the Aillik Group have suggested its deposition on top of the NAC and above or adjacent to the IHBPS in a back-arc/rifted arc basin or retro-arc foreland basin (Moumblow *et al.*, 2019 and references therein; Ketchum *et al.*, 2002). Nevertheless, several lines of evidence, including structural geology, geochronology, and isotopic and geochemistry data, indicate an outboard origin of the Aillik Group above a continental crust younger than the reworked Archean crust of the Kaipokok Domain (Culshaw *et al.*, 2000; Hinchey, 2021b, c). Therefore, direct sourcing from the exposed or underlying basement related to the Kaipokok Domain into the Aillik basin is considered unlikely.

More recent tectonic models propose ongoing subduction beneath the Aillik basin (*e.g.*, Aillik–Cape Harrison Arc) before its collision with the established Kaipokok Domain (Hinchey *et al.*, 2023). During this subduction, sediments derived from the Kaipokok Domain could have been subducted and integrated into the mantle wedge of the Aillik–Cape Harrison Arc.

Zircon, as a resistant and refractory mineral, can survive the temperature and pressure conditions of the mantle wedge (Bea *et al.*, 2018; Cambeses *et al.*, 2023). Subducted zircons that resurfaced as xenocrysts in mantle peridotites in back-arc regions (Liu *et al.*, 2009; Proenza *et al.*, 2018), and in volcanic and plutonic rocks of continental and oceanic arcs (*e.g.*, Sunda Arc and the Cretaceous Caribbean Island arc; Rojas-Agramonte *et al.*, 2016; Torró *et al.*, 2018; Gao *et al.*, 2022) attest to the capability of zircon grains to survive in hot, zircon-undersaturated environments for an extended period of time (tens of millions of years; Siebel *et al.*, 2009; Rojas-Agramonte *et al.*, 2017).

Thus, it is possible that zircons derived from the Kaipokok Domain were subducted and later resurfaced as xenocrysts in volcanic and plutonic rocks of the Aillik Group. Indeed, the inherited Archean (2914–2717 Ma) zircons in the Aillik volcanic and plutonic rocks (LaFlamme *et al.*, 2013; Hinchey *et al.*, 2020), which are older than the calculated $T_{(DM)}$ model ages for the Aillik crust (LaFlamme *et al.*, 2013; Hinchey, 2021b), may represent this process. Based on the near-source nature of the sediments (*e.g.*, poor compositional maturity and sorting), the geochemical signature indicating mainly felsic volcanic provenance, and the absence of metamorphic clasts (Hinchey, 2021a), the Archean (older than 2773 Ma) and some Paleoproterozoic (2100–1900 Ma) zircons in the Aillik Group sedimentary rocks are interpreted as xenocrysts that were eroded from local volcanic and plutonic rocks, rather than direct sourcing from exposed or underlying NAC basement.

The detrital zircon U–Pb age data from the Aillik Group strata shows an increase in older ages towards the top of the stratigraphic sequence (Figure 3A, B). This suggests a change in sediment sources over time, where the earlier part of the sequence was dominated by local felsic volcanic sources, but was later replaced by a mixed source consisting of both the local felsic volcanic rocks and an older sialic basement. This change in provenance likely reflects a period of increased tectonic activity, which resulted in the reworking of the Aillik Group strata (Figure 7) and the exhumation of the Aillik basement. This interpretation is further supported by the presence of sedimentary, volcanic, and granite clasts in the conglomerates observed in the upper parts of the stratigraphic sequence (columns A-B, as described in Hinchey, 2021a).

TECTONIC IMPLICATIONS

Previous sedimentological and geochemical studies on the sedimentary and volcanic rocks of the Aillik Group suggest that sedimentation and volcanism occurred in an extensional back-arc basin setting between approximately 1883 and 1848 Ma (Hinchey, 2021a, c). The detrital age spectra of the Aillik Group sedimentary rocks contain a high proportion of detrital zircons with crystallization ages (CA) close to the depositional age (DA) of the unit (maximum depositional age of *ca.* 1843 Ma), with 55% of the zircon population plotting within CA–DA <100 Ma (Figure 9). This age distribution is consistent with deposition in a convergent tectonic setting (Cawood *et al.*, 2012). Sedimentation within a fore-arc usually exhibits a unimodal zircon distribution related to the nearby magmatic activity, whereas back-arc settings exhibit increased input from older detritus derived from adjacent cratons or exhumed crustal basement (Cawood *et al.*, 2012). The Aillik Group sedimentary rocks display a polymodal zircon distribution, with older age peaks attributed to basement sources. This zircon distribution pattern coincides with the expected signature for sediments deposited in a back-arc basin setting. In summary, the detrital zircon age data, combined with the previous sedimentological and geochemical evidence, supports the interpretation that the Aillik Group sedimentary rocks were deposited in an extensional back-arc basin between *ca.* 1883 and 1848 Ma.

The absence of the regional D_2 compressional fabric of the Kaipokok Domain within the Aillik Group coupled with juvenile isotopic data support a Neoarchean/Paleoproterozoic (2770–2160 Ma) basement for the Aillik

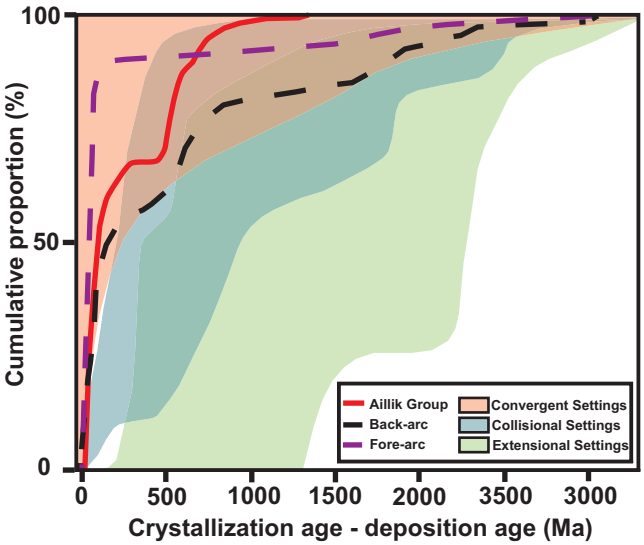

Figure 9. *Tectonic setting diagram for detrital zircons from the Aillik Group sedimentary rocks. Modified from Cawood* et al. *(2012).*

Group and suggests an allochthonous origin for the Aillik back-arc (Hinchey, 2021b). This back-arc is thought to have formed on the substrate of a continental arc, referred to as the Cape Harrison arc/microcontinent, which laid outboard from the already stablished Kaipokok Domain (Hinchey *et al.*, 2023). The detrital zircon age data provides further support for this interpretation. There is little to no presence of detrital zircons derived from the NAC, and a high proportion of zircon ages that overlap the calculated Nd model ages ($T_{(DM)}$) for the Aillik sialic basement (2770–2160 Ma; Hinchey, 2021b). This suggests that the sediment sources for the Aillik Group were derived from a basement that is younger than the NAC and the reworked (*ca.* 2878–2813 Ma) Archean gneisses of the Kaipokok Domain (Ketchum *et al.*, 2002). These results challenge the proximity of a basement of the NAC or Kaipokok Domain during the deposition of the Aillik Group and support the hypothesis that the Aillik Group basement had an allochthonous origin.

The accretion of the Aillik–Cape Harrison Arc to the Kaipokok Domain occurred after 1848 Ma, based on the youngest age of felsic volcanism in the Aillik Group (Hinchey *et al.*, 2020) and possibly after 1836 Ma, based on a break-in igneous activity in Ketilidian orogen (Vestergaard *et al.*, 2024). The new provenance data, presented herein, indicates that Aillik magmatism continued at least until *ca.* 1843 Ma, when a shift in sediment provenance indicates a change in tectonic activity. Specifically, the provenance changed from being dominated by syn-depositional, felsic volcanic rocks to a mixed source of older basement and syn-depositional, felsic volcanic rocks.

Sedimentation was continuous as no unconformities were identified in the Aillik Group stratigraphy (Hinchey, 2021a), thus the observed change in detrital provenance likely represents continuous unroofing, related to the progressive inversion of the Aillik basin before its detachment and northwest-directed (present-day coordinates) thrusting over the Kaipokok Arc. This occurred along a series of thrust faults, including the Kaipokok Bay, the Big Island, the Pomiadluk Point and Double Island shear zones (Hinchey, 2013, 2021d; Culshaw *et al.*, 2000). Available geochronology data from the Kaipokok Bay Shear Zone suggest that localized sillimanite-grade metamorphism and dextral transpression occurred at 1841 ± 2 Ma (Ketchum *et al.*, 1997). The overlap between this metamorphic age and the calculated MDA for the Aillik Group sedimentary rocks (1843 ± 2Ma) supports the interpretation of coeval metamorphism and basin inversion, which is consistent with the oblique accretion of the Aillik–Cape Harrison Arc to the assembled Kaipokok Domain. The timing of correlative events in the Ketilidian orogen are thought to be younger, *ca.* 1836 (Bagas *et al.*, 2020), based on the gap in magmatic activity in the Julianehåb Igneous Complex, our results could indi-

cate that the arc-continent collision along the Makkovik–Ketilidian orogen was diachronous, with the accretion of the Aillik–Cape Harrison Arc occurring slightly earlier than the accretion in the Ketilidian orogen.

CONCLUSIONS

1) The new provenance data from the Aillik Group sedimentary rocks support the interpretation that sedimentation occurred in a back-arc basin. The sediments were primarily sourced from local Paleoproterozoic felsic volcanic rocks and a Paleoproterozoic to Neoarchean sialic basement that is younger than the NAC or the reworked Archean crust within the Kaipokok Domain.

2) MDA results for the Aillik sedimentary rocks suggest that magmatism and back-arc extension continued until at least *ca.* 1843 Ma. Following this, oblique accretion of the Aillik–Cape Harrison Arc to the assembled Kaipokok Domain began.

3) The change in the Aillik sedimentary rock provenance, from being dominated by Paleoproterozoic sources to a mixed source containing both Paleoproterozoic and Neoarchean sources, records the progressive inversion of the Aillik basin during the onset of the collision.

4) The overlap between the MDA calculation for the Aillik sedimentary rocks (1843 ± 2 Ma) and the timing of sillimanite-grade metamorphism recorded in the Kaipokok Shear Zone (1841 ± 2 Ma) may indicate that the onset of the collision between the Aillik–Cape Harrison Arc and the assembled Kaipokok Domain occurred between 1843–1841 Ma.

REFERENCES

Allaart, J.H.
1976: Ketilidian mobile belt in South Greenland. *In* Geology of Greenland. *Edited by* A. Escher and W.S. Watt. Geological Survey of Denmark and Greenland, pages 120-151. https://doi.org/10.22008/gpub/38212

Bagas, L., Kolb, J., Nielsen, T.F.D. and Groves, D.I.
2020: The complex tectonic evolution of the craton-adjacent northern margin of the Palaeoproterozoic Ketilidian Orogen, southeastern Greenland: Evidence from the geochemistry of mafic to intermediate and granitic intrusions. Lithos, Volume 358-359, pages 1-21. https://doi.org/10.1016/j.lithos.2020.105384

Barham, M., Kirkland, C.L. and Handoko, A.D.
2022: Understanding ancient tectonic settings through detrital zircon analysis. Earth and Planetary Science Letters, Volume 583, pages 1-10. https://doi.org/10.1016/j.epsl.2022.117425

Barr, S., White, C.E., Culshaw, N.G. and Ketchum, J.W.F.
2001: Geology and tectonic setting of Paleoproterozoic granitoid suites in the Island Harbour Bay area, Makkovik Province, Labrador. Canadian Journal of Earth Sciences, Volume 38(3), pages 441-463. https://doi.org/10.1139/e00-086

Bea, F., Montero, P. and Palma, J.F.M.
2018: Experimental evidence for the preservation of U-Pb isotope ratios in mantle-recycled crustal zircon grains. Scientific Reports, Volume 8(12904), pages 1-10. https://doi.org/10.1038/s41598-018-30934-4

Bhatia, M.R. and Crook, K.A.W.
1986: Trace element characteristics of graywackes and tectonic setting discrimination of sedimentary basins. Contributions to Mineralogy and Petrology, Volume 92(2), pages 181-193. https://doi.org/10.1007/BF00375292

Cambeses, A., Chakraborty, S., Jöns, N., Montero, P. and Bea, F.
2023: How does inherited zircon survive in partially molten mantle: Insights on modes of magma transport in the mantle from nanoscale melt-crystal interaction experiments. Earth and Planetary Science Letters, Volume 601, pages 1-13. https://doi.org/10.1016/j.epsl.2022.117911

Cawood, P.A., Hawkesworth, C.J. and Dhuime, B.
2012: Detrital zircon record and tectonic setting. Geology, Volume 40(10), pages 875-878. https://doi.org/10.1130/g32945.1

Condie, K.C.
1993: Chemical composition and evolution of the upper continental crust: contrasting results from surface samples and shales. Chemical Geology, Volume 104, pages 1-37.

Condie, K.C. and Wronkiewicz, D.J.
1990: The Cr/Th ratio in Precambrian pelites from the Kaapvaal Craton as an index of craton evolution. Earth and Planetary Science Letters, Volume 97(3), pages 256-267. https://doi.org/10.1016/0012-821X(90)90046-Z

Cox, R.A., Lowe, D.R. and Cullers, R.L.
1995: The influence of sediment recycling and basement composition on evolution of mudrock chemistry in the southwestern United States. Geochimica et

Cosmochimica Acta, Volume 59(14), pages 2919-2940. https://doi.org/10.1016/0016-7037(95)00185-9

Cox, R.A., Wilton, D.H.C. and Kosler, J.
2003: Laser-ablation U-Th-Pb in siu dating of zircon and allanite: An example from October Harbour Granite, central coast Labrador, Canada. The Canadian Mineralogist, Volume 41(2), pages 273-291. https://doi.org/10.2113/gscanmin.41.2.273

Cullers, R.L.
1994: The controls on the major and trace element variation of shales, siltstones, and sandstones of Pennsylvanian-Permian age from uplifted continental blocks in Colorado to platform sediment in Kansas, USA. Geochimica et Cosmochimica Acta, Volume 58(22), pages 4955-4972. https://doi.org/10.1016/0016-7037(94)90224-0

2000: The geochemistry of shales, siltstones and sandstones of Pennsylvanian–Permian age, Colorado, USA: Implications for provenance and metamorphic studies. Lithos, Volume 51(3), pages 181-203. https://doi.org/10.1016/S0024-4937(99)00063-8

Cullers, R.L., Basu, A. and Suttner, L.J.
1988: Geochemical signature of provenance in sand-size material in soils and stream sediments near the Tobacco Root batholith, Montana, U.S.A. Chemical Geology, Volume 70(4), pages 335-348. https://doi.org/10.1016/0009-2541(88)90123-4

Cullers, R.L., Bock, B. and Guidotti, C.
1997: Elemental distributions and neodymium isotopic compositions of Silurian metasediments, western Maine, USA: Redistribution of the rare earth elements. Geochimica et Cosmochimica Acta, Volume 61(9), pages 1847-1861. https://doi.org/10.1016/S0016-7037(97)00048-3

Cullers, R.L. and Podkovyrov, V.N.
2000: Geochemistry of the Mesoproterozoic Lakhanda shales in southeastern Yakutia, Russia: Implications for mineralogical and provenance control, and recycling. Precambrian Research, Volume 104(1), pages 77-93. https://doi.org/10.1016/S0301-9268(00)00090-5

Culshaw, N., Ketchum, J. and Barr, S.
2000: Structural evolution of the Makkovik Province, Labrador, Canada: Tectonic processes during 200 Myr at a Paleoproterozoic active margin. Tectonics, Volume 19, pages 961-977.

Ermanovics, I.
1993: Geology of Hopedale Block, southern Nain Province, and the adjacent Proterozoic terranes, Labrador, Newfoundland. Geological Survey of Canada, Memoir 431, 161 pages. https://doi.org/10.4095/183986

Fedo, C.M., Nesbitt, H.W. and Young, G.M.
1995: Unraveling the effects of potassium metasomatism in sedimentary rocks and paleosols, with implications for paleoweathering conditions and provenance. Geology, Volume 23(10), pages 921-924. https://doi.org/10.1130/0091-7613(1995)023<0921:UTEOPM>2.3.CO;2

Finch, C., Roldan, R., Walsh, L., Kelly, J. and Amor, S.
2018: Analytical methods for chemical analysis of geological materials. Government of Newfoundland and Labrador, Department of Natural Resources, Geological Survey, Open File NFLD/3316, 67 pages.

Floyd, P.A. and Leveridge, B.E.
1987: Tectonic environment of the Devonian Gramscatho basin, south Cornwall: Framework mode and geochemical evidence from turbiditic sandstones. Journal of the Geological Society, Volume 144(4), pages 531-542. https://doi.org/10.1144/gsjgs.144.4.0531

Folk, R.L.
1951: Stages of textural maturity in sedimentary rocks. Journal of Sedimentary Research, Volume 21(3), pages 127-130. https://doi.org/10.2110/jsr.21.127

1980: Petrology of Sedimentary Rocks. Hemphill Publishing Company, 179 pages.

Gale, A., Dalton, C.A., Langmuir, C.H., Su, Y. and Schilling, J.
2013: The mean composition of ocean ridge basalts. Geochemistry, Geophysics, Geosystems, Volume 14, Issue 33, pages 489-518. https://doi.org/10.1029/2012GC004334

Gao, M.-H., Liu, P.-P., Chung, S.-L., Li, Q.-L., Wang, B., Tian, W., Li, X.-H. and Lee, H.-Y.
2022: Himalayan zircons resurface in Sumatran arc volcanoes through sediment recycling. Communications Earth and Environment, Volume 3, Article 283, 11 pages. https://doi.org/10.1038/s43247-022-00611-6

Giovanoli, R., Schnoor, J.L., Sigg, L., Stumm, W. and Zobrist, J.
1988: Chemical weathering of crystalline rocks in the catchment area of acidic Ticino Lakes, Switzerland. Clays and Clay Minerals, Volume 36(6), pages 521-529. https://doi.org/10.1346/CCMN.1988.0360605

Gower, C. and Ryan, A.
1986: Proterozoic evolution of the Grenville Province and adjacent Makkovik Province in eastern-central Labrador. *In* The Grenville Province. *Edited by* J.M. Moore, A. Davidson, and A.J. Baer. Geological Association of Canada, Special Paper 31, pages 281-296.

Herron, M.M.
1988: Geochemical classification of terrigenous sands and shales from core or log data. Journal of Sedimentary Research, Volume 58(5), pages 820-829. https://doi.org/10.1306/212f8e77-2b24-11d7-8648000102c1865d

Hinchey, A.M.
2013: Geology of the Makkovik area, Labrador (NTS 13O/03 and parts of NTS 13O/02). Map 2013-07, Scale 1:50 000. Government of Newfoundland and Labrador, Department of Natural Resources, Geological Survey, Open File 013O/0138.

2021a: Lithofacies architecture and paleoenvironment of a Paleoproterozoic volcano-sedimentary sequence: Insight into rift-related volcanism during supercontinent assembly. Precambrian Research, Volume 367, pages 1-22. https://doi.org/10.1016/j.precamres.2021.106443

2021b: Lithogeochemical and Nd isotopic constraints on felsic magmatism in the Makkovik Orogen, Labrador, Canada: Implications for assembly of the supercontinent Nuna. Lithos, Volume 382-383. https://doi.org/10.1016/j.lithos.2020.105917

2021c: Localized backarc extension in an overall compressional setting during the assembly of Nuna: Geochemical and isotopic evidence from Orosirian (1883–1848 Ma) mafic magmatism of the Aillik Group, Labrador, Canada. Earth and Space Science, Volume 8(6). https://doi.org/10.1029/2020EA001489

2021d: Reply to Dickin (2021) comment(s) on Hinchey (2021): "Lithogeochemical and Nd isotopic constraints on felsic magmatism in the Makkovik Orogen, Labrador, Canada: Implications for assembly of the supercontinent Nuna". Lithos, Volume 392-393. https://doi.org/10.1016/j.lithos.2021.106158

Hinchey, A., Butler, J.P. and Serna Ortiz, S.
2022: Island Harbour Bay Plutonic Suite, Labrador. *In* Current Research. Government of Newfoundland and Labrador, Department of Industry, Energy and Technology, Geological Survey, Report 22-1, pages 147-156.

Hinchey, A., Rayner, N. and Davis, W.J.
2020: Episodic Paleoproterozoic crustal growth preserved in the Aillik Domain, Makkovik Province, Labrador. Precambrian Research, Volume 337. https://doi.org/10.1016/j.precamres.2019.105526

Hinchey, A., Sandeman, H.A. and Butler, J.P.
2023: The Paleoproterozoic granite factory: Voluminous post-collisional, ferroan, A-type granites and implications for crust formation and metallogenic tenor, Labrador, Canada. Geological Society of America, Bulletin, 136(1-2), pages 893-916. https://doi.org/10.1130/b36727.1

Hu, P.-y., Zhai, Q.-g., Cawood, P. A., Weinberg, R. F., Zhao, G.-c., Tang, Y. and Liu, Y.-m.
2023: Paleogeographic reconstruction of Precambrian terranes reworked by Phanerozoic orogens: An example based on detrital zircon REE from Lhasa Terrane in southern Tibet. Geophysical Research Letters, Volume 50(5). https://doi.org/10.1029/2023GL102979

Hubert, J.F.
1962: A zircon-tourmaline-rutile maturity index and the interdependence of the composition of heavy mineral assemblages with the gross composition and texture of sandstones. Journal of Sedimentary Research, Volume 32, pages 440-450.

Kerr, A.
1994: Early Proterozoic magmatic suites of the eastern Central Mineral Belt (Makkovik Province), Labrador: Geology, geochemistry and mineral potential. Government of Newfoundland and Labrador, Department of Natural Resources, Geological Survey, Report 94-03, 167 pages.

Kerr, A., Ryan, B., Gower, C.F. and Wardle, R.J.
1996: The Makkovik Province: Extension of the Ketilidian Mobile Belt in mainland North America. Geological Society, London, Special Publications, Volume 112(1), pages 155-177. https://doi.org/10.1144/GSL.SP.1996.112.01.09

Ketchum, J.W.F., Culshaw, N.G. and Barr, S.M.
2002: Anatomy and orogenic history of a Paleoproterozoic accretionary belt: The Makkovik Province, Labrador, Canada. Canadian Journal of Earth Sciences, Volume 39(5), pages 711-730. https://doi.org/10.1139/e01-099

Ketchum, J.W.F., Dunning, G.R. and Culshaw, N.G.
1997: U–Pb geochronologic constraints on Paleoproterozoic orogenesis in the northwestern Makkovik Province, Labrador, Canada. Canadian Journal of Earth Sciences, Volume 34(8), pages 1072-1088. https://doi.org/10.1139/e17-087

Ketchum, J.W.F., Jackson, S.E., Culshaw, N.G. and Barr, S.M.
2001: Depositional and tectonic setting of the Paleoproterozoic Lower Aillik Group, Makkovik Province, Canada: Evolution of a passive margin-foredeep sequence based on petrochemistry and U–Pb (TIMS and LAM-ICP-MS) geochronology. Precambrian Research, Volume 105(2), pages 331-356. https://doi.org/10.1016/S0301-9268(00)00118-2

Košler, J., Fonneland, H., Sylvester, P., Tubrett, M. and Pedersen, R.
2002: U–Pb dating of detrital zircons for sediment provenance studies—a comparison of laser ablation ICPMS and SIMS techniques. Chemical Geology, Volume 182(2), pages 605-618. https://doi.org/10.1016/S0009-2541(01)00341-2

LaFlamme, C., Sylvester, P. J., Hinchey, A.M. and Davis, W.J.
2013: U–Pb age and Hf-isotope geochemistry of zircon from felsic volcanic rocks of the Paleoproterozoic Aillik Group, Makkovik Province, Labrador. Precambrian Research, Volume 224, pagse 129-142. https://doi.org/10.1016/j.precamres.2012.09.005

Liu, Y., Gao, S., Hu, Z., Gao, C., Zong, K. and Wang, D.
2009: Continental and oceanic crust recycling-induced melt–peridotite interactions in the Trans-North China Orogen: U–Pb dating, Hf isotopes and trace elements in zircons from mantle xenoliths. Journal of Petrology, Volume 51(1-2), pages 537-571. https://doi.org/10.1093/petrology/egp082

MacLean, W.H. and Kranidiotis, P.
1987: Immobile elements as monitors of mass transfer in hydrothermal alteration; Phelps Dodge massive sulfide deposit, Matagami, Quebec. Economic Geology, Volume 82(4), pages 951-962. https://doi.org/10.2113/gsecongeo.82.4.951

McLennan, S.M., Hemming, S., McDaniel, D.K. and Hanson, G. N.
1993: Geochemical approaches to sedimentation, provenance, and tectonics. *In* Processes Controlling the Composition of Clastic Sediments. *Edited by* M.J. Johnsson and A. Basu. Geological Society of America. https://doi.org/10.1130/SPE284-p21

McLennan, S.M. and Taylor, S.R.
1991: Sedimentary rocks and crustal evolution: Tectonic setting and secular trends. The Journal of Geology, Volume 99(1). https://doi.org/10.1086/629470

Moumblow, R.M., Arcuri, G.A., Dickin, A.P. and Gower, C.F.
2019: Nd and Pb isotope mapping of crustal domains within the Makkovik Province, Labrador. Geological Magazine, Volume 156(5), pages 833-848. https://doi.org/10.1017/S0016756818000195

Namayandeh, A., Modabberi, S. and López-Galindo, A.
2020: Trace and rare earth element distribution and mobility during diagenetic alteration of volcanic ash to bentonite in eastern Iranian bentonite deposits. Clays and Clay Minerals, Volume 68(1), pages 50-66. https://doi.org/10.1007/s42860-019-00054-9

Nelson, D.R.
2001: An assessment of the determination of depositional ages for precambrian clastic sedimentary rocks by U–Pb dating of detrital zircons. Sedimentary Geology, Volume 141-142, pages 37-60. https://doi.org/10.1016/S0037-0738(01)00067-7

Nesbitt, H.W. and Young, G.M.
1982: Early Proterozoic climates and plate motions inferred from major element chemistry of lutites. Nature, Volume 299(5885), pages 715-717. https://doi.org/10.1038/299715a0

1984: Prediction of some weathering trends of plutonic and volcanic rocks based on thermodynamic and kinetic considerations. Geochimica et Cosmochimica Acta, Volume 48(7), pages 1523-1534. https://doi.org/10.1016/0016-7037(84)90408-3

Pettijohn, F.J., Potter, P.E. and Siever, R.
1987: Sand and Sandstone (Second ed.). Springer-verlag, New York, 553 pages.

Potter, P.E.
1978: Petrology and chemistry of modern big river sands. The Journal of Geology, Volume 86(4), pages 423-449. https://doi.org/10.1086/649711

Proenza, J.A., González-Jiménez, J.M., Garcia-Casco, A., Belousova, E., Griffin, W.L., Talavera, C., Rojas-Agramonte, Y., Aiglsperger, T., Navarro-Ciurana, D., Pujol-Solà, N., Gervilla, F., O'Reilly, S.Y. and Jacob, D.E.
2018: Cold plumes trigger contamination of oceanic mantle wedges with continental crust-derived sediments: Evidence from chromitite zircon grains of eastern Cuban ophiolites. Geoscience Frontiers, Volume 9(6), pages 1921-1936. https://doi.org/10.1016/j.gsf.2017.12.005

Rojas-Agramonte, Y., Garcia-Casco, A., Kemp, A., Kröner, A., Proenza, J.A., Lázaro, C. and Liu, D.
2016: Recycling and transport of continental material through the mantle wedge above subduction zones: A Caribbean example. Earth and Planetary Science Letters, Volume 436, pages 93-107. https://doi.org/10.1016/j.epsl.2015.11.040

Rojas-Agramonte, Y., Williams, I.S., Arculus, R., Kröner, A., García-Casco, A., Lázaro, C., Buhre, S., Wong, J., Geng, H., Echeverría, C., Jeffries, T., Xie, H. and Mertz-Kraus, R.
2017: Ancient xenocrystic zircon in young volcanic rocks of the southern Lesser Antilles island arc. Lithos, Volume 290-291, pages 228-252. https://doi.org/10.1016/j.lithos.2017.08.002

Rollinson, H.R.
1993: Using Geochemical Data: Evaluation, Presentation, Interpretation (1st ed.). Routledge. https://doi.org/10.4324/9781315845548

Roser, B.P. and Korsch, R.J.
1986: Determination of tectonic setting of sandstone-mudstone suites using SiO_2 content and K_2O/Na_2O ratio. The Journal of Geology, Volume 94(5), pages 635-650. https://doi.org/10.1086/629071

Rothfuss, J.L., Lielke, K. and Weislogel, A.L.
2012: Application of detrital zircon provenance in paleogeographic reconstruction of an intermontane basin system, Paleogene Renova Formation, southwest Montana. *In* Mineralogical and Geochemical Approaches to Provenance. *Edited by* E.T. Rasbury, S.R. Hemming and N.R. Riggs. Geological Society of America. https://doi.org/10.1130/2012.2487(04)

Rudnick, R.L. and Gao, S.
2003: The Composition of the Continental Crust. *In* Treatise on Geochemistry. *Edited by* H.D. Holland and K.K. Turekian. Elsevier-Pergamon, Oxford, Volume (3): The Crust, pages 1-64. http://dx.doi.org/10.1016/b0-08-043751-6/03016-4

Sen, S. and Mishra, M.
2023: Implications of heavy mineral assemblage to sediment recycling, rare earth element budget and provenance of Kaimur sandstones, Vindhyan Supergroup, Son Valley. Journal of Earth System Science, Volume 132(1). https://doi.org/10.1007/s12040-022-02013-w

Shi, C., Yan, M. and Chi, Q.
2011: Abundances of chemical elements in granitoids of different geological ages and their characteristics in China. Geoscience Frontiers, Volume 2(2), pages 261-275. https://doi.org/10.1016/j.gsf.2011.02.002

Siebel, W., Schmitt, A.K., Danišík, M., Chen, F., Meier, S., Weiß, S., and Eroğlu, S.
2009: Prolonged mantle residence of zircon xenocrysts from the western Eger rift. Nature Geoscience, Volume 2(12), pages 886-890. https://doi.org/10.1038/ngeo695

Sláma, J., Košler, J., Condon, D., Crowley, J.L., Gerdes, A., Hanchar, J.M., Horstwood, M.S.A., Morris, G., Nasdala, L., Norberg, N., Schaltegger, U., Schoene, B., Tubrett, M.N. and Whitehouse, M.J.
2008: Plešovice zircon — A new natural reference material for U–Pb and Hf isotopic microanalysis. Chemical Geology, Volume 249(1). https://doi.org/10.1016/j.chemgeo.2007.11.005

Steenfelt, A., Kolb, J. and Thrane, K.
2016: Metallogeny of South Greenland: A review of geological evolution, mineral occurrences and geochemical exploration data. Ore Geology Reviews, Volume 77, pages 194-245. https://doi.org/10.1016/j.oregeorev.2016.02.005

Stern, R.A.
1997: The GSC Sensitive High Resolution Ion Microprobe (SHRIMP): analytical techniques of zircon U-Th-Pb age determinations and performance evaluation. In Current Research. Geological Survey of Canada, Report 1997-F. https://doi.org/10.4095/209089

Stern, R.A. and Amelin, Y.
2003: Assessment of errors in SIMS zircon U–Pb geochronology using a natural zircon standard and NIST SRM 610 glass. Chemical Geology, Volume 197(1), pages 111-142. https://doi.org/10.1016/S0009-2541(02)00320-0

Sylvester, P. and Ghaderi, M.
1997: Trace element analysis of scheelite by excimer laser ablation-inductively coupled plasma-mass spec-

trometry (ELA-ICP-MS) using a synthetic silicate glass standard. Chemical Geology, Volume 141(1), pages 49-65. https://doi.org/10.1016/S0009-2541(97)00057-0

Sun, S.S. and McDonough, W.F.
1989: Chemical and isotopic systema-tics of oceanic basalts: implications for mantle compositionand processes. *In* Magmatismin the Ocean Basins. *Edited by* A.D. Saunders and M.J. Norry. Geological Society, London, Special Publications, Volume 42, pages 313-345.

Torró, L., Proenza, J. A., Rojas-Agramonte, Y., Garcia-Casco, A., Yang, J.-H. and Yang, Y.-H.
2018: Recycling in the subduction factory: Archaean to Permian zircons in the oceanic Cretaceous Caribbean island-arc (Hispaniola). Gondwana Research, Volume 54, pages 23-37.
https://doi.org/10.1016/j.gr.2017.09.010

Vermeesch, P.
2021: Maximum depositional age estimation revisited. Geoscience Frontiers, Volume 12(2), pages 843-850. https://doi.org/10.1016/j.gsf.2020.08.008

Vestergaard, R., Waight, T., Petersson, A., Hinchey, A.M. and Whitehouse, M.J.
2024: A Paleoproterozoic magmatic flare-up in the Central Domain of the Ketilidian Orogen, South Greenland, and correlations to Canada and Scandinavia. Precambrian Research, Volume 403.
https://doi.org/10.1016/j.precamres.2024.107320

Wiedenbeck, M., Allé, P., Corfu, F., Griffin, W.L., Meier, M., Oberli, F., Quadt, A.V., Roddick, J.C. and Spiegel, W.
1995: Tree natural zircon standards for U-Th-Pb, Lu-Hf, Trace element and REE analyses. Geostandards Newsletter, Volume 19(1).
https://doi.org/10.1111/j.1751-908X.1995.tb00147.x